



## Machine learning-guided optimization, predictive modeling, and experimental validation of MXene-based supercapacitors



Anjali R. Shelake<sup>a</sup>, Vijay C. Karade<sup>c</sup>, Manickam Selvaraj<sup>d,e,\*</sup>, Mohammed A. Assiri<sup>d,e</sup>, Dipti D. More<sup>a</sup>, Amruta D. Patil<sup>a</sup>, Mukund G. Mali<sup>f</sup>, Santosh S. Sutar<sup>g,\*\*</sup>, Rutuja U. Amate<sup>h,\*\*\*</sup>, Chan-Wook Jeon<sup>h,\*\*\*\*</sup>, Tae Geun Kim<sup>i,\*\*\*\*\*</sup>, Tukaram D. Dongale<sup>a,b,i,\*\*\*\*\*</sup>

<sup>a</sup> Computational Electronics and Nanoscience Research Laboratory, School of Nanoscience and Biotechnology, Shivaji University, Kolhapur, 416004, Maharashtra, India

<sup>b</sup> Functional Materials and Materials Chemistry Laboratory, Department of Physiology, Saveetha Dental College & Hospitals, Saveetha Institute of Medical & Technical Sciences, Saveetha University, Chennai, 600077, Tamil Nadu, India

<sup>c</sup> Wright Center for Photovoltaics Innovation and Commercialization, Department of Physics and Astronomy, University of Toledo, Toledo, OH, 43606, USA

<sup>d</sup> Department of Chemistry, Faculty of Science, King Khalid University, Abha, 61413, Saudi Arabia

<sup>e</sup> Research Centre for Advanced Materials Science (RCAMS), King Khalid University, AlQura'a, P.O. Box 960, Abha, Saudi Arabia

<sup>f</sup> School of Chemical Sciences, Purnyashlok Ahilyadevi Holkar Solapur University, Solapur, 413255, India

<sup>g</sup> Yashwantrao Chavan School of Rural Development, Shivaji University, Kolhapur, 416004, Maharashtra, India

<sup>h</sup> School of Chemical Engineering, Yeungnam University, 280 Daehak-ro, Gyeongsan, 712-749, Republic of Korea

<sup>i</sup> School of Electrical Engineering, Korea University, Anam-ro 145, Seongbuk-gu, Seoul, Republic of Korea

\* Corresponding authors. Department of Chemistry, Faculty of Science, King Khalid University, Abha, 61413, Saudi Arabia.

\*\* Corresponding authors.

\*\*\* Corresponding authors.

\*\*\*\* Corresponding author.

\*\*\*\*\* Corresponding author.

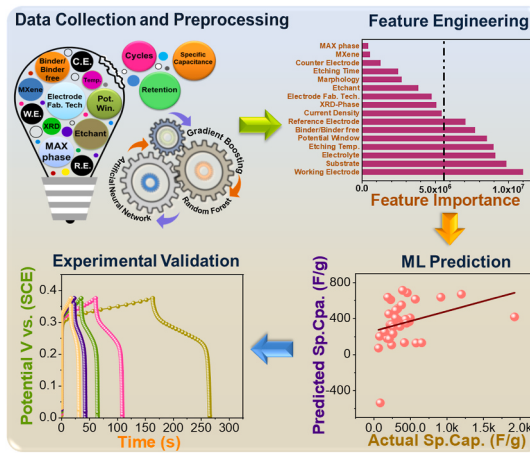
\*\*\*\*\* Corresponding author. Computational Electronics and Nanoscience Research Laboratory, School of Nanoscience and Biotechnology, Shivaji University, Kolhapur, 416004, Maharashtra, India.

E-mail addresses: [msselvaraj@kku.edu.sa](mailto:msselvaraj@kku.edu.sa) (M. Selvaraj), [sss.ycsrd@unishivaji.ac.in](mailto:sss.ycsrd@unishivaji.ac.in) (S.S. Sutar), [rutu.nanoworld@gmail.com](mailto:rutu.nanoworld@gmail.com) (R.U. Amate), [cwjjeon@ynu.ac.kr](mailto:cwjjeon@ynu.ac.kr) (C.-W. Jeon), [tgkim1@korea.ac.kr](mailto:tgkim1@korea.ac.kr) (T.G. Kim), [tdd.snst@unishivaji.ac.in](mailto:tdd.snst@unishivaji.ac.in) (T.D. Dongale).

## HIGHLIGHTS

- Machine learning framework to identify key parameters affecting MXene-based supercapacitor (SC) performance.
- The CART algorithm was utilized to gain electrochemical insights into MXene-based supercapacitors.
- Predicted output performance (specific capacitance, cyclic stability, and capacitive retention) using various ML algorithms.
- Identified key parameters in synthesis, fabrication, and electrochemical testing that influence SC performance.
- Experimental validation for both the GCD and CV models showed good agreement with the ML-predicted results.

## GRAPHICAL ABSTRACT



## ARTICLE INFO

**Keywords:**  
Machine learning  
MXene  
Supercapacitor  
2D materials  
Energy storage

## ABSTRACT

In the present work, we extracted approximately 7,500 data points related to MXene-based supercapacitors (SCs) from the existing literature and categorized them based on galvanostatic charge-discharge (GCD) and cyclic voltammetry (CV) measurements. The datasets are analyzed using classification and regression trees to gain electrochemical insights. The feature importance analysis revealed that the working electrode's material composition, substrate, electrolyte, counter electrode, etching time, etchant, fabrication technique, potential window, and current density are the most influential parameters governing the SC performance. Moreover, different ML algorithms such as random forest (RF), artificial neural network (ANN), gradient boosting (GB), and linear model (LM) are utilized to predict the specific capacitance, cyclic stability, and capacitive retention of MXene-based SCs. Among them, RF showed the highest predictive accuracy (Pearson's  $r \approx 0.94$ , Adj.  $R^2 \approx 0.88$ ), outperforming GB ( $r \approx 0.56$ ,  $R^2 \approx 0.31$ ), ANN ( $r \approx 0.44$ ,  $R^2 \approx 0.17$ ), and LM ( $r \approx 0.29$ ,  $R^2 \approx 0.06$ ) across both CV and GCD datasets. The optimized ML model achieved prominent prediction accuracy, suggesting strong agreement with reported experimental data. This study offers a reliable and efficient approach to optimizing MXene-based SCs and accelerates the design of advanced materials for energy storage applications.

## 1. Introduction

With the rapid depletion of fossil fuel reserves and growing concerns about environmental challenges, there is an urgent need to explore sustainable and clean renewable energy sources [1,2]. Developing and utilizing these energy alternatives has become critical for addressing global energy demands and mitigating environmental impacts [3]. Accordingly, energy storage technologies like supercapacitors (SCs) have received wide attention due to their exceptional characteristics, including rapid power delivery, outstanding rate performance, and prolonged cyclic stability [4–6]. Given these facts, new materials have been developed by researchers to improve the charge storage capability of SCs. These materials include but are not limited to metal-organic frameworks (MOFs) [7,8], black phosphorus [9], and polyoxometalates [10]. However, these two-dimensional (2D) materials often exhibit poor electrochemical performance, cause deficiencies in charge storage, and are prone to degradation [11]. In recent years, a new type of 2D material, MXene, has been widely employed for various electronic device applications, which was discovered by Prof. Yury Gogotsi and his colleagues in 2011 [12–15].

MXene represents a large family of 2D layered materials with the general formula  $M_{n+1}X_nTx$ , where M refers to early transition metals, x represents carbides, nitrides, or carbonitrides ( $n = 1$  to 3), and Tx denotes terminating groups (-O, -OH, -F) [16,17]. MXenes have emerged as promising pseudocapacitive electrode materials due to their high conductivity, surface group adjustability, large specific surface area,

structural stability, large interlayer spacing, etc. [18–20]. Considering a variation of elements and surface functional groups, the thickness of a single layer is controlled by several metal layers in the MAX phase (precursor), and various types of MXene [21]. These changes in the elements and structural diversities of MXene cause significant variations in their electronic structures, which are crucial for improving pseudocapacitive performance. Moreover, the large number of structural and elemental variables makes it challenging yet substantial to identify the meaningful factors for designing efficient pseudocapacitive electrode materials [19,22,23]. Generally, investigations of MXene have primarily focused on titanium-based MXene, which is highly impactful due to its pseudocapacitance mechanism. Furthermore, certain experimental conditions have shown that the specific capacitance of MXene can be enhanced by reducing surface groups, ion adsorption, diffusion, and charge transfer [24–28]. Therefore, to identify the influencing parameters and reduce the overall cost of experimentation, it is advisable to use high-throughput, machine learning (ML)-based analysis techniques.

The fundamental principle underlying ML schemes is to gather all relevant features/variables of a candidate material to analyze and study the relationships between the physical, chemical, and electrochemical properties of materials with their corresponding output performance variables. In the case of SCs, cyclic stability, capacitive retention, and specific capacitance are the output performance features. Generally, ML models, when applied to material science, provide an effective and accurate means of predicting material properties, a capability that has proven transformative in recent years [29,30]. This emerging

technology, particularly within the last decade, has significantly advanced our ability to predict and optimize material behaviors, thereby improving accuracy, reducing time spent in experimentation, and enabling more effective exploration of materials' energy characteristics [31–33]. Moreover, ML algorithms can identify key parameters in the device fabrication process, which allows for the elimination of redundant or excessive steps in fabrication, optimizing both the efficiency and cost-effectiveness of the production process. As a result, ML has become a powerful tool for enhancing the design and performance of materials.

The MXene SCs show enhanced performance with low fabrication cost and ease of synthesis [34]. However, the primary obstacle lies in the optimization of fabrication techniques, which requires meticulous fine-tuning of parameters to achieve desired performance metrics. Despite advancements in the field, the lack of standardized protocols often compels researchers to engage in a trial-and-error approach. This

not only consumes valuable time but also demands extensive resources, particularly for those working with novel materials or pioneering unconventional methodologies. In addition to fabrication challenges, the synthesis and electrochemical characterization of materials present another critical bottleneck in developing materials with the requisite properties for energy storage applications, often involving complex and iterative processes. These include material selection, chemical synthesis, structural modification, and ensuring compatibility with device configurations. Consequently, early-stage researchers often find themselves dedicating an inordinate amount of time to these preliminary stages, potentially diverting focus from broader scientific inquiries or innovative applications. The above-mentioned hurdles can be overcome by employing ML approaches, which can reduce the overall cost of experimentation. In the past, different materials were analyzed with the help of ML algorithms for SC applications. However, these studies mainly fall

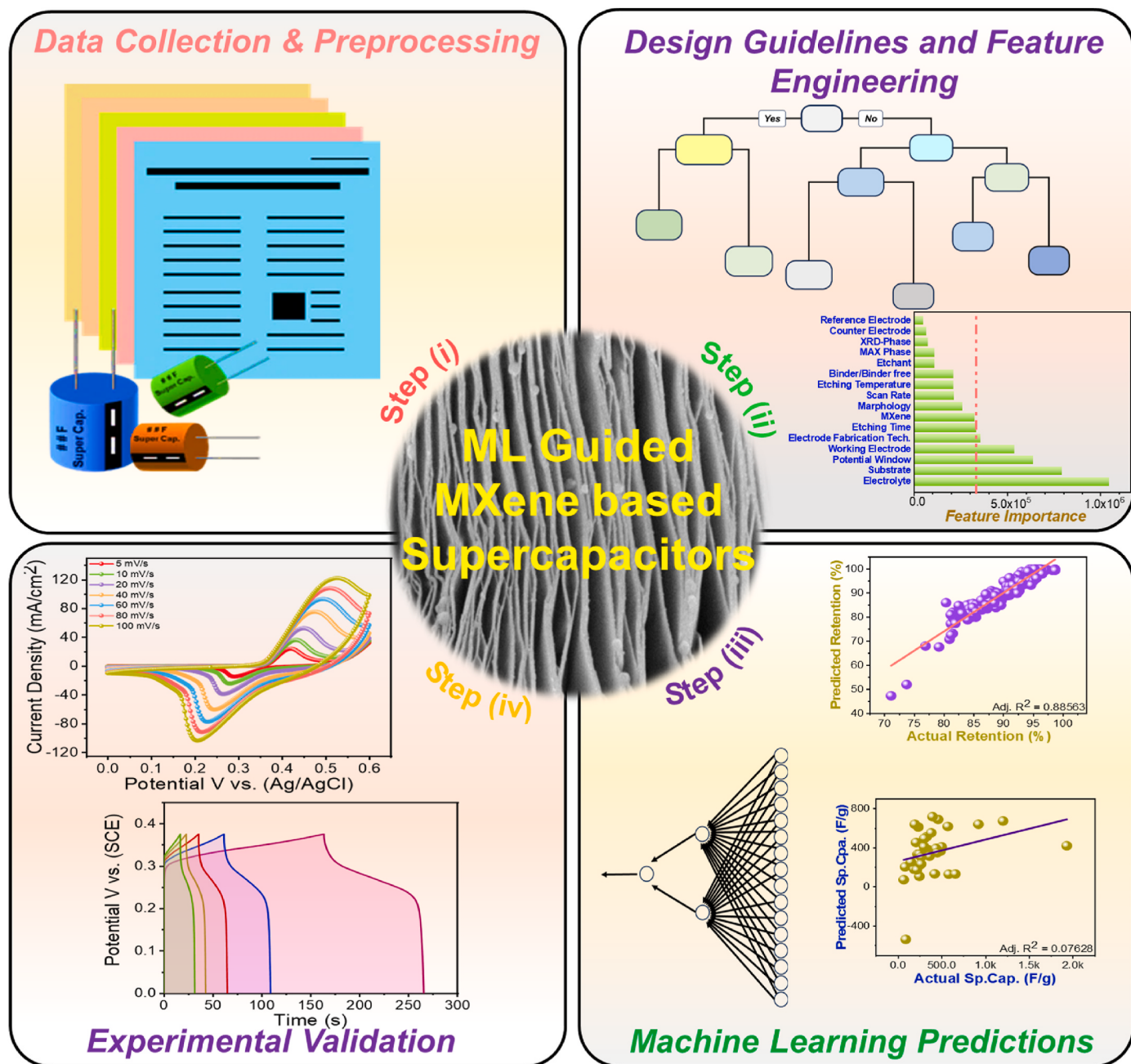


**Fig. 1.** Illustration of an ML-guided approach for the optimization and prediction of MXene-based SCs. First, data was collected, cleaned, and encoded. Next, optimization, prediction, and feature engineering were performed. Finally, the ML results were experimentally validated.

back in several aspects, viz., i) minimum data points were used to train the models, and ii) the least number of input and output variables were analyzed [35,36]. To tackle these issues, the ML-guided models for SCs should be based on a large number of datasets. Additionally, the models should be built on key parameters of the synthesis and electrode fabrication conditions. In the case of MXene-based SCs, very few ML studies have contributed to understanding their charge storage properties and device optimizations.

Considering the previously reported ML studies and inspired by the above-mentioned insights, in the present work, we developed ML models for high-performance MXene-based SCs. The typical workflow is shown in Fig. 1. For building ML models, we collected data points from previously reported peer-reviewed literature. After collecting raw data from the literature, the datasets were divided into two types, i.e., Galvanostatic charge-discharge (GCD) and cyclic voltammetry (CV). This step is important because most of the researchers either employed the GCD technique or the CV technique for the calculation of specific capacitance. For optimization, prediction, and feature engineering purposes, various ML algorithms such as classification and regression tree (CART), random forest (RF), artificial neural network (ANN), linear model (LM), and gradient boosting (GB) were utilized. Finally, the ML predictions were validated through the fabrication of MXene-based SCs.

The present finding suggested that ML is an effective approach to optimize and develop high-performance MXene-based SCs. In particular, the present work offers data-driven insights into the correlations of synthesis, fabrication, and electrochemical parameters in MXene-based SCs. The ML-assisted CART and feature importance analyses reveal that material composition of the working electrode, fabrication technique, MXene etching time, substrate conductivity, electrolyte composition, counter electrode, potential window, and current density critically modulate specific capacitance, cycle stability, and capacitive retention. These insights could enable the rational optimization of MXene structures for enhanced energy and power densities. As a result, the proposed ML framework can accelerate the discovery of high-performance MXene-based SCs and also contribute to the understanding of the electrochemical performance of MXene-based nanomaterials.

## 2. Methodology

### 2.1. Dataset preparation

In the present ML work, a dataset comprising approximately 7500 data points was compiled from experimental results reported in studies focusing on MXene and its composite electrodes applied for SC applications. The SC performance data was mainly collected based on GCD and CV results. The dataset was divided into two groups based on the synthesis, electrode fabrication, and electrochemical measurement methods that are employed to calculate specific capacitance. The CV and GCD techniques can provide different specific capacitance values for the same device, owing to their charge storage properties in an applied potential window, scan rate, and current density. In the case of CV, the specific capacitance can be calculated using the area under the curve, while the discharging time is utilized in the GCD technique. To address missing information, domain expertise was systematically employed to infer and complete the missing data points. To tabulate data points, the following input parameters were used: MAX phase, type of MXene, etchant, etching time (hrs), etching temperature (°C), type of composite, phase of materials, morphology, electrode fabrication technique, substrates, electrolytes, binder/binder-free, type of working electrode (WE), counter electrode (CE), and reference electrode (RE), potential window (PW), scan rate (SR, mV/s), current density (Cd, A/g). The specific capacitance (F/g), cyclic stability (%), and capacitive retention (%) are the output parameters of the ML models. The detailed information on categorical and continuous input and output features present in the GCD and CV datasets is summarized in Tables S1 and S2, respectively. Therefore, categorical features are coded using numerical values for

better handling during CART implementation, predictions, and feature engineering. Apart from the above-mentioned features/variables, the electrode thickness, mass loading, active surface area, pore size, Coulombic efficiency, and information related to the electrochemical impedance spectroscopy (EIS) are not fully described in the reported research papers. Considering this, we have excluded these parameters from the present ML study. It is important to note that some features frequently appeared across multiple data points, and we acknowledge the possibility of bias. In particular, the over-representation of  $Ti_3C_2T_x$ -type MXene, HF etchant, and doctor blade/brush coating techniques may have influenced the overall feature weighting in the ML models. In the case of ML predictions, we employed a cross-validation technique to ensure that no single parameter or material disproportionality affected the model predictions. Moreover, the heterogeneity of the dataset was maintained by sourcing data from various peer-reviewed journals representing different laboratories and countries.

### 2.2. Computational details

The primary objectives of the present ML study are to investigate (i) how input parameters affect the electrochemical performance of MXene-based SCs, (ii) which major features/variables affect the specific capacitance, cyclic stability, and capacitive retention of MXene-based SCs, and (iii) which ML models are best suited for the predictions of output performance of the MXene-based SCs, as both datasets are very heterogeneous in nature. In the present work, the CART algorithm was employed to predict synthesis and fabrication guidelines and establish rules from both GCD and CV datasets for high-performance MXene-based SCs. The material properties, synthesis conditions, structural and morphological attributes, electrode fabrication parameters, and electrochemical testing parameters were used as input features in the CART model and provided quantitative decision rules for output performance features (specific capacitance, cyclic stability, and capacitive retention) to optimize high-performance MXene-based SCs. The RF, GB, ANN, and LM algorithms were used to predict the output performance of MXene-based SCs. Similar to CART, these predictive algorithms were trained based on input features and provided the corresponding output performance. The models were trained using 80 % data, while 20 % data was used for testing purposes. The effectiveness of the models was assessed using Adj.  $R^2$  and Pearson's correlation values. The feature importance for both datasets (GCD and CV) was modeled using the RF algorithm. All machine learning models were scripted in R Studio (R version 3.6.2). The statistical analysis was performed using MS Excel, and Origin 2018 was used for the plotting of the graphs.

## 3. Results and discussion

### 3.1. Statistical analysis

The present research aims to achieve high-performance MXene-based SCs driven by ML with optimum feature parameters. Under the ML study, we examined a diverse set of MXenes with different chemical compositions [3,37,38]. In formulating effective ML models, the size, quality, and quantity of data majorly decide the success of the model, followed by independent and dependent variables [39]. Accordingly, input features of two datasets (GCD and CV) are summarized in Supporting Tables S1 and S2, encompassing potential causal factors that influence the output features, such as specific capacitance, stability, and capacitive retention. The input features can be categorized into material properties, synthesis conditions, structural and morphological attributes, electrode fabrication parameters, and electrochemical testing parameters. These input and output features were graphically presented in Figs. S1 and S2 (Supporting Information). Moreover, their summary description is outlined in the Supporting Information (Notes 1, 2, and 3).

### 3.2. Design guidelines formulated using CART-based ML algorithms

We initially used the CART algorithm to unravel the electrochemical insights of MXene-based SCs based on the GCD dataset. The dataset comprised intrinsic numerical and categorical (coded into numerical form) features, making CART an appropriate choice for handling such heterogeneous datasets. Herein, the primary objective is to develop an optimization model that is capable of accurately estimating important performance output properties of MXene-based SCs. This estimation was based on a range of input features such as type of MAX phase, MXene, and etchant, etching time, etching temperature, type of composite, structural and morphological characteristics, electrode fabrication technique, substrates, electrolytes, binder/binder-free electrode, type of working electrode (WE), counter electrode (CE) and reference electrode (RE), potential window, and current density. In the case of the CV-based dataset, the scan rate was utilized as an input feature in place of the current density.

Fig. 2 suggests several representative decision rules in a CART model of specific capacitance. Generally, the CART model consists of two types of nodes (root node and leaf node), which play an important role in the decision process. The decision rules are displayed at the bottom of each node. From the CART model, we observed that the root node divides into two parts with low specific capacitance (yes side) and high specific capacitance (no side). The first decision rule present at the root node suggested that if a WE is fabricated using bare MXene and some composites (MXene-metal oxide/hydroxide, MXene-carbon, MXene-polymer), an average specific capacitance of 441 F/g can be achieved. Conversely, if we fabricate a WE with composite materials like MXene-selenides, MXene-sulfides, MXene-fluorides, MXene-LDHs, and doped-MXene, then we can achieve a specific capacitance of 858 F/g. This variation in specific capacitance is attributed to the charge storage properties of the material under investigation, and it is influenced by the interplay of various electrochemical parameters during the analysis of SCs [40]. Moreover, the specific capacitance is predominantly governed by the mass loading on the active surface area and pore size, which plays a critical role in determining the overall electrochemical performance

[41]. The CART model further provides a decision rule for high specific capacitance. For instance, the CART suggested that if we fabricate a WE with alkalinized MXene-metal, MXene-cellulose nanofiber, MXene-lignin derivatives, MXene-cyanuric acid, MXene-chitin, MXene-biomass derived carbon fibers, etc., then we can achieve an average specific capacitance of 1106 F/g [42,43]. In addition to WE materials, if we use SCE, Hg/HgO, Hg/Hg<sub>2</sub>SO<sub>4</sub>, and Hg/HgCl<sub>2</sub> as REs, then a specific capacitance improved to 1284 F/g. The CART model also predicts that the highest specific capacitance of 1513 F/g can be achieved if the operational PW is maintained within a specific range (1 to -1 V and 0 to 1 V). This change in specific capacitance occurs because RE, such as SCE, Hg/HgO, Hg/Hg<sub>2</sub>SO<sub>4</sub>, and Hg/HgCl<sub>2</sub> can stabilize the electrode potential during electrochemical measurements. This stabilization ensures consistent and accurate potential control, leading to improved charge storage and, consequently, higher specific capacitance. Moreover, when we adjust the specific ranges of PW (+1 to -1 V and 0 to +1 V), it can significantly impact the electrochemical performance of MXene-based electrodes. An optimized PW allows for the full utilization of the material's redox-active sites, enhancing pseudocapacitive behavior and increasing specific capacitance [44].

The CART model for cyclic stability and capacitive retention is represented in Fig. S3a and S3b, respectively (Supporting Information). The decision rules of cyclic stability suggested that, if we use platinum as CE during electrochemical testing, we get an average of 7800 cycles of stability. On the other hand, the cyclic stability of 22,000 cycles can be achieved if we employ activated carbon, carbon rods, graphite rods, and YP-50 as CE with substrates like fiber-based substrates, ITO, gold-coated PET, polymer-based porous membranes, natural rubber foam/cellulose nanofibers/wood/water permeable membrane, titanium foil/mesh, etc. (Fig. S3a). The CART model further suggests that achieving cyclic stability beyond 10,000 cycles is possible by optimizing the type and concentration of the electrolyte and maintaining the etching temperature <30 °C. Tailoring the electrolyte composition improves electrode wettability, which facilitates efficient ion transport and reduces interfacial resistance factors that are crucial for achieving long-term cycling stability. Similarly, precise control over etching temperatures during

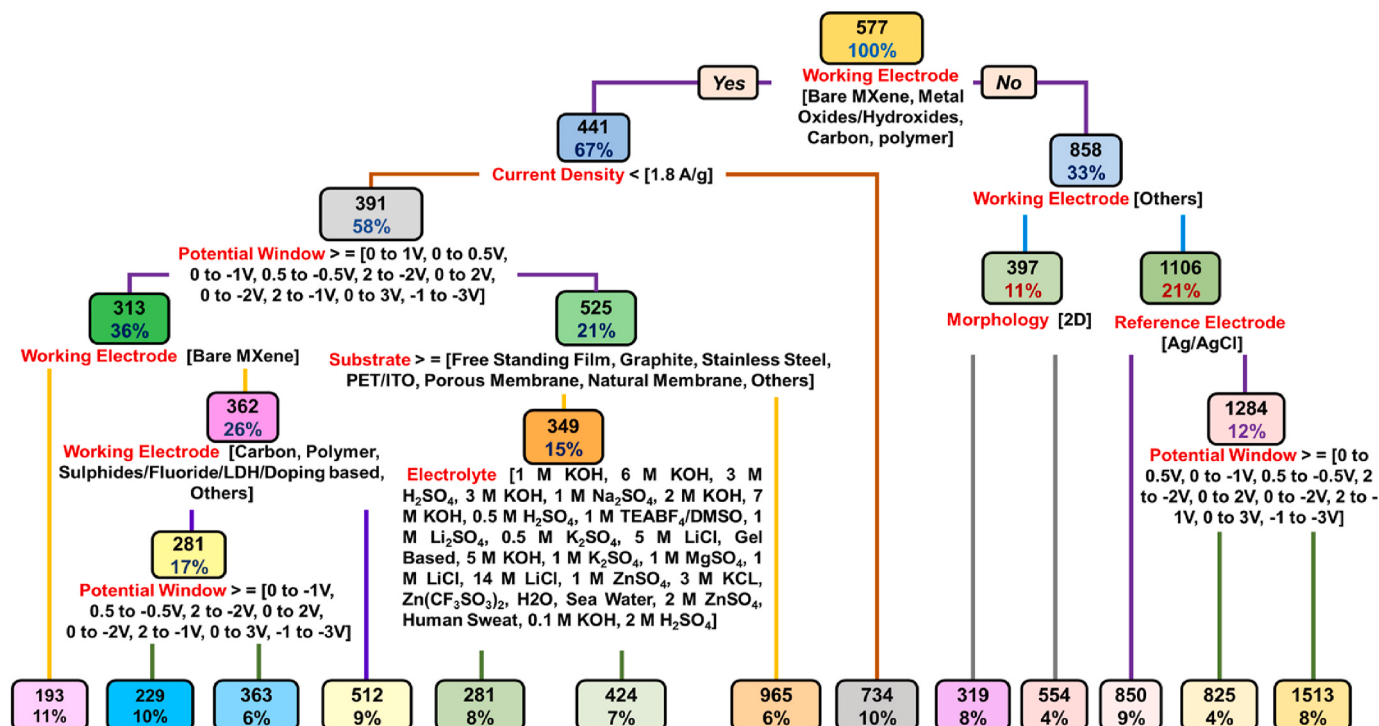


Fig. 2. CART-based ML predictive model for the specific capacitance of MXene-based SCs. The present model is developed using the GCD dataset.

electrode preparation can refine surface morphology, promoting uniform electrochemical activity and mitigating degradation over extended cycles. Accordingly, engineering and selection of WE materials directly influence structural integrity, electrochemical stability and extending the device's lifespan. Advanced fabrication methods enable the production of electrodes with controlled architectures and compositions, contributing to enhanced durability and performance. Collectively, these strategies address the long life span of cyclic stability.

The CART model for capacitive retention underlines the importance of CE as the root decision rule (Fig. S3b). Under this framework, if we use CE apart from platinum and maintain PWs like +0.5 to -0.5 V, +2 to -2, 0 to +2 V, 0 to -2 V, -1 to +2 V, 0 to +3 V, and -1 to -3 V, then 96 % capacitance can be retained in the MXene-based SCs. Moreover, optimized capacitance retention can be achieved by carefully selecting suitable binders, maintaining the etching temperature <43 °C, and controlling the morphology and electrode fabrication techniques. If we select proper binders, it ensures better adhesion of MXene layers, reducing contact resistance and preventing structural degradation. Simultaneously, factors like etching temperature significantly affect the morphology and interlayer spacing of MXene, also impacting ion accessibility and electrolyte penetration. Moreover, an optimized electrode fabrication technique enhances electrochemical stability by minimizing mechanical stress and maintaining electrode integrity over cycling. These factors collectively contribute to prolonged cycling stability and improved capacitance retention. The CV-based CART models of specific capacitance, cycle stability, and capacitive retention of MXene-based SCs are shown in Fig. S4a–c (Supporting Information). A detailed explanation of these CART models is summarized in a supporting information file. The model highlights that optimized PW, binder-free electrodes, and choice of electrode fabrication techniques

influence the specific capacitance, cyclic stability, and capacitive retention of MXene-based SCs [45,46].

### 3.3. Impact of features on specific capacitance, cycle stability, and capacitive retention of MXene-based SCs (GCD dataset)

In this section, we investigated how individual input parameters (features) affect the output performance of the MXene-based SCs. The feature importance score also provides the significant input features that directly affect the SC performance. Therefore, this study can help us provide valuable insights for ranking input features based on their significance. Fig. 3a–c represents the feature importance score of specific capacitance, cyclic stability, and capacitive retention of MXene-based SCs. In this section, we have utilized the GCD dataset of the MXene-based SCs. The feature importance analysis of specific capacitance, cyclic stability, and capacitive retention of MXene-based SCs based on the CV dataset is shown in Fig. 4. Fig. 3a shows the feature importance plot of specific capacitance, suggesting that the WE is the most important input feature that affects the overall capacitance of MXene-based SCs. In addition to these features, the choice of substrate, electrolyte, etching temperature, potential window, binder/binder-free electrodes, and reference electrode influences the specific capacitance of MXene-based SCs [47]. The remaining features have the least impact on the capacitance of the MXene-based SCs. Fig. 3b represents the features that predominantly contribute to cyclic stability. The choice of electrolytes, substrate, counter electrodes, binder/binder-free electrodes, and etchant decides the cyclic stability of the MXene-based SCs. The other features have the least impact on cyclic stability performance. Fig. 3c shows the feature importance score that influences capacitive retention. In this case, the etching time has the greatest impact on the specific

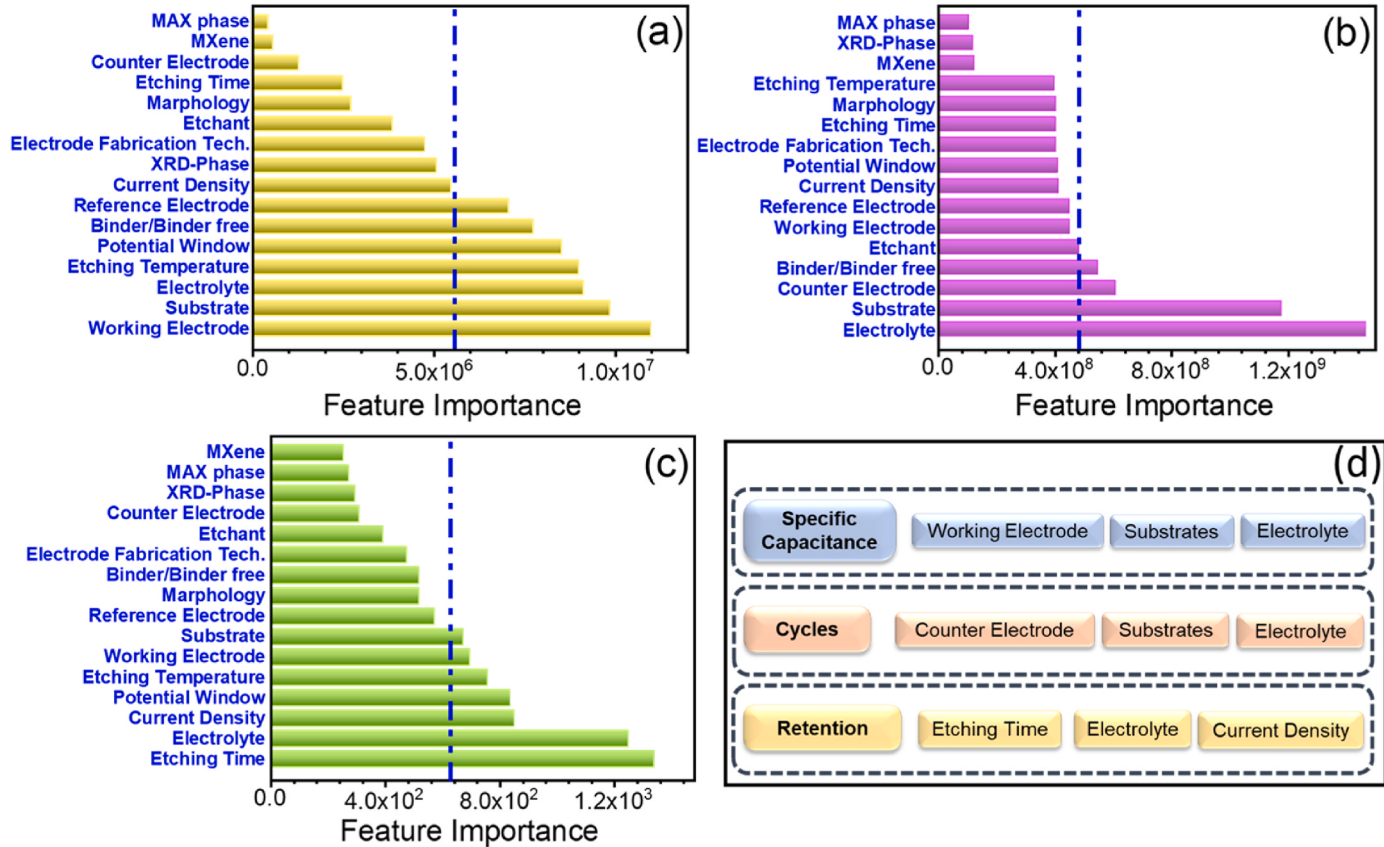


**Fig. 3.** Feature importance score of MXene SCs (GCD dataset). The feature importance of (a) specific capacitance, (b) cyclic stability, and (c) capacitive retention. (d) List of three significant features that influence the performance of MXene-based SCs. The group average (vertical lines) is calculated to make a threshold boundary for analysis purposes.

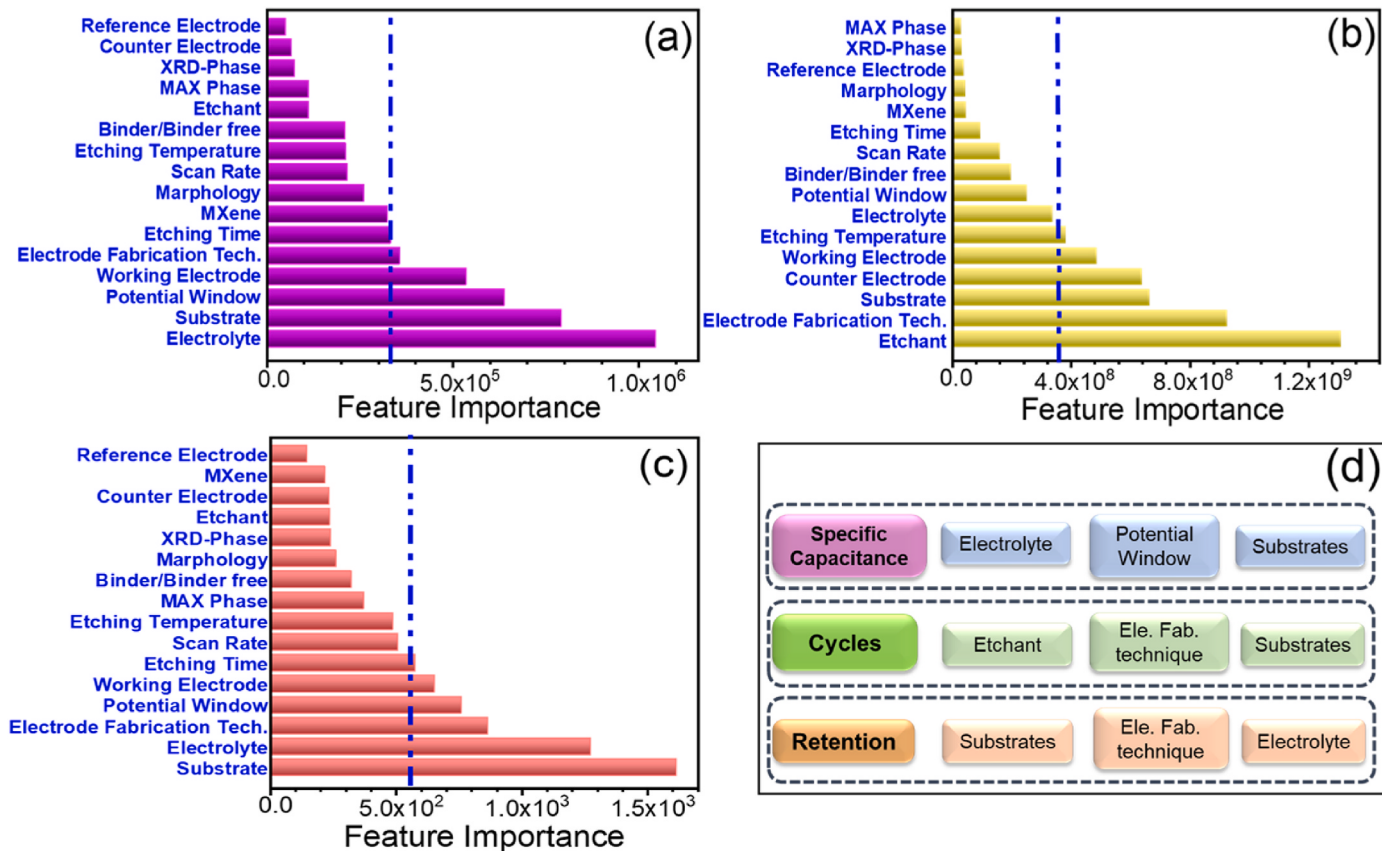


**Fig. 4.** Feature importance score of MXene-based SCs (CV dataset). The feature importance of (a) specific capacitance, (b) cyclic stability, and (c) capacitive retention. (d) List of three significant features that influence the performance of MXene-based SCs. The group average (vertical lines) is calculated to make a threshold boundary for analysis purposes.

capacitance. Additionally, the choice of electrolytes, current density, potential window, etching temperature, working electrodes and substrates also influences the capacitive retention of MXene-based SCs. The list of three significant features affecting the electrochemical behavior of MXene-based SCs based on the GCD dataset is shown in Fig. 3d. In the present study, the feature importance analysis of the GCD dataset reveals that the material composition of the working electrode, substrate, and electrolyte, along with the type of counter electrode, MXene etching time, and current density, are the key determinants of SC performance.

Generally, etching time is an important factor in the synthesis of MXene. An increase in etching time results in MXene with larger encircled CV curves and a more symmetrical shape than other prepared MXene, suggesting a higher specific capacitance and greater electrochemical activity of the electrode. This phenomenon is primarily attributed to a higher carbon content, which enhances electronic conductivity, and a relatively larger specific surface area, allowing better access of the aqueous electrolyte to the electrode [48]. Moreover, the working electrode plays a crucial role in enhancing supercapacitor performance by determining the device's energy storage capacity, power output, and cycling stability. Its material composition, surface morphology, porosity, and electrical conductivity directly influence charge storage mechanisms, whether through electric double-layer capacitance (EDLC) or pseudocapacitance. High-surface-area nanostructured materials, such as carbon-based materials (e.g., graphene, carbon nanotubes), metal oxides (e.g.,  $\text{MnO}_2$ ,  $\text{RuO}_2$ ), and conductive polymers, improve charge accumulation and ion diffusion [49]. The MXene-based composites are excellent electrode materials for SCs, owing to their outstanding electrical conductivity, diverse oxidation states, and superior electrochemical activity [50–56]. The synergistic effects of MXene-based composites can enhance reversible redox

reactions with high capacity and stable cycling performance for extended duration. In addition to this, the MXene-biomass derived carbon composites possess excellent electrical conductivity, and abundant redox active sites that promote fast charge transfer and reversible faradaic reactions [51]. Unlike the other carbon materials, the biomass-derived carbon materials inherit the unique structure, defects, and chemical compositions of biomass precursors. Therefore, resulting biomass-derived carbon materials and composites deliver high specific capacitance and improved rate capability, and excellent cycling performance due to their extremely high surface area, hierarchical porosity, and abundant functional groups, which improve electrolyte accessibility and ion diffusion [51,54].

Additionally, electrode-electrolyte interactions further enhance performance by reducing resistance and improving charge transfer kinetics. Furthermore, modifying the working electrode's structure and composition can significantly boost capacitance and rate capability [6]. The aqueous electrolyte is a majorly utilized feature in electrochemical characterization, compared to ionic and solid electrolytes [57]. The main advantage of aqueous electrolytes is that they contain different concentrations of cations, which influence the electrode-electrolyte interface at the surface of the electrode. This phenomenon prominently helps during cyclic stability [58]. The choice of substrate plays an important role in identifying the electrochemical performance of supercapacitors by influencing charge transport, electrode adhesion, and overall cyclic stability. Conductive substrates such as carbon cloth, nickel foam, and stainless-steel mesh provide high electrical conductivity, facilitating efficient electron transfer and reducing internal resistance [59]. Flexible substrates like graphene films and polymer-based materials enhance mechanical stability and enable wearable energy storage applications. Additionally, porous and

three-dimensional substrates offer increased surface area, improving electrolyte accessibility and ion diffusion, leading to higher capacitance and better rate capability. Optimizing substrate properties can significantly enhance supercapacitor efficiency, making them suitable for diverse applications [60]. Accordingly, the current density influences the charge storage capacity, rate capability, etc. At lower current densities, supercapacitors exhibit higher specific capacitance due to sufficient ion diffusion and charge accumulation at the electrode-electrolyte interface. However, at higher current densities, rapid charge-discharge rates enhance power density but may lead to reduced capacitance due to diffusion limitations and increased internal resistance. Generally, the counter electrode maintains charge balance and enables efficient electrochemical reactions. Eventually, it serves as a reference for electron flow, ensuring a stable potential difference during charge-discharge cycles. The choice of counter-electrode material significantly influences capacitance, energy density, and cycling stability. Highly conductive and electrochemically stable materials, such as platinum, carbon-based electrodes, or transition metal oxides, improve ion transport and reduce internal resistance, enhancing overall device performance. The selection of an appropriate potential window influences the performance of supercapacitors by directly affecting their energy storage capacity. However, expanding the potential window requires careful optimization to prevent electrolyte decomposition and electrode degradation, which can lead to capacity fading and a reduced lifespan [61]. The choice of electrolyte and electrode material compatibility is essential in defining a stable and optimal operating potential range, electrochemical stability, and cycle life. A wider potential window enables higher energy and power density [62]. The binder is a significant feature for improving the performance of SCs, as it acts as a bridge between the electrode material substrates. The best binder can prevent materials from peeling off during electrode operation, providing excellent cyclic stability, capacitive retention, specific capacitance, and good mechanical properties [63,64]. Furthermore, etching temperature is another reliable feature to enhance the performance of MXene-based electrodes. According to previous reports, a mixture of mixed acids or low concentrations of HF acid under thermal conditions is prominently utilized for MXene synthesis because it reduces defect density in the synthesized MXene. Additionally, it exfoliates the compact structure of the MAX phase and easily removes the A layer from the MAX phase, which contributes to stability [65,66].

Additionally, we developed another feature importance ranking for MXene-based SCs based on the CV dataset, as depicted in Fig. 4a–d. In this case, sixteen key features were analyzed, which directly influence the output performance parameters of SCs. In this case, the specific capacitance is influenced by the choice of substrate, electrolyte, potential window, working electrode, electrode fabrication technique, and etching time (Fig. 4a). The remaining features have the lowest feature importance score; therefore, these features have a relatively small effect on the specific capacitance of MXene-based SCs. In the case of cyclic stability, Etchant, electrode fabrication technique, substrates, counter electrode, working electrode, and etching temperature can influence the cyclic stability of MXene-based SCs (Fig. 4b). In the case of capacitance retention, substrate, electrolyte, electrode fabrication technique, potential window, working electrode, and etching time have the most influence (Fig. 4c). In summary, the CV dataset suggested that the substrate, electrolyte, etchant, electrode fabrication technique, potential window, working electrode, and counter-electrode features govern the electrochemical behavior of MXene-based SCs (Fig. 4d).

#### 3.4. Prediction of specific capacitance, cycle stability, and capacitive retention of MXene-based SCs

In the next phase, for the prediction of specific capacitance, cycle stability, and capacitive retention of MXene-based SCs, we employed four major algorithms, i.e., RF, GB, ANN, and LM. The ANN is a unique ML algorithm, inspired by biological neural networks, and it is

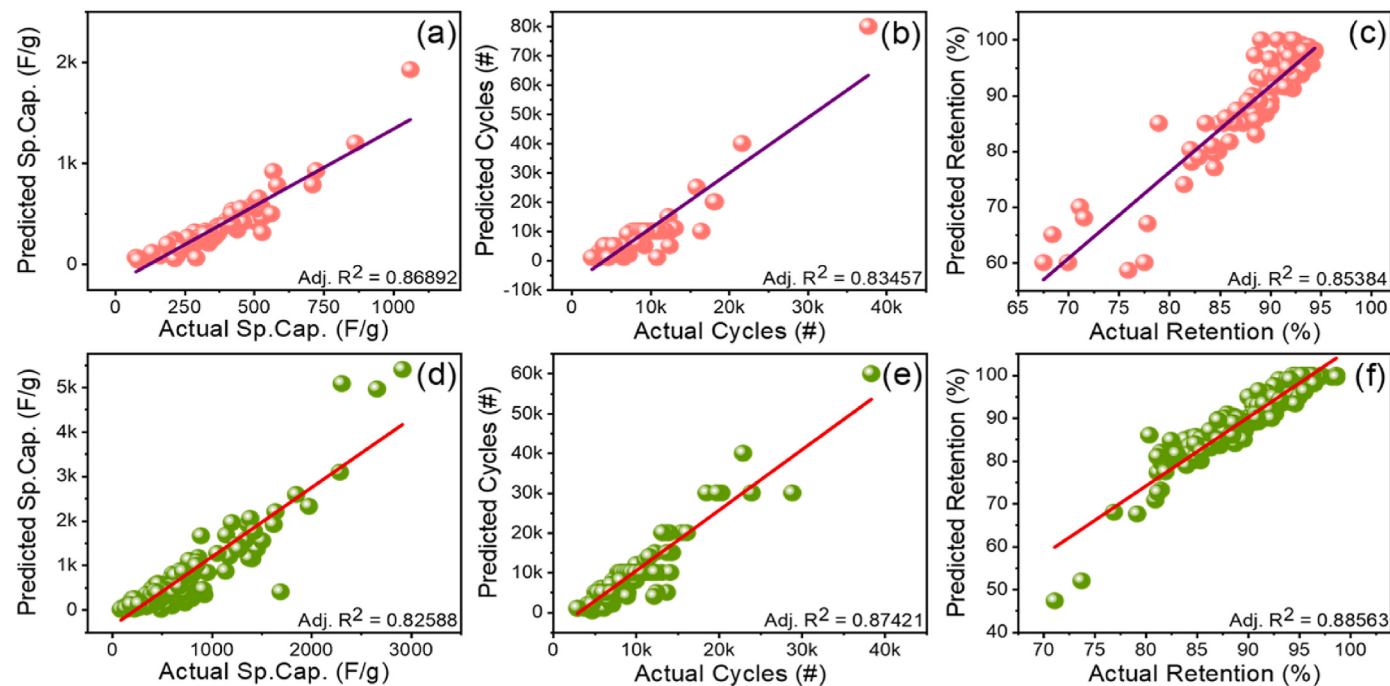
recommended for the prediction of highly nonlinear data. LM is a regression-based algorithm that can also predict complex datasets [67, 68]. We also utilized the GB algorithm to predict and estimate continuous output features, focusing on its speed and accuracy [69]. RF is a group-based linear regression and utilizes multiple classifiers to solve complex problems. In the proposed models, we incorporated a random sampling technique [70] and a cross-validation technique for model-building purposes. The models were trained using 80 % data, while 20 % data was used for testing purposes. The test data were used to evaluate the performance of these models. The effectiveness of the models was assessed using Adj.  $R^2$  and Pearson's correlation values.

Fig. 5a–f represents a scatter plot of actual and predicted values of the specific capacitance, cyclic stability, and capacitive retention of the MXene-based SCs using the RF algorithm. The scatter plots of GB, ANN, and LM algorithms, containing actual and predicted specific capacitance, cyclic stability, and capacitive retention based on GCD and CV datasets, are shown in Figs. S5, S6, and S7, respectively. The statistical measures, such as Pearson's  $r$  and Adj.  $R^2$  values of each predictive algorithm are summarized in Table S3. The prediction results suggested that the only RF algorithm effectively predicts output performance parameters of MXene-based SCs. The remaining predictive algorithms failed to predict the specific capacitance, cyclic stability, and capacitive retention of the MXene-based SCs (Table S3 and Figs. S5, S6, and S7). The RF algorithm is an ensemble of decision trees, which is robust to noise, less sensitive to hyperparameter tuning, and effectively handles high-dimensional data with multicollinearity. On the other hand, the ANN required extensive parameter optimization and balanced training samples to achieve stable convergence, which is difficult in such a heterogeneous dataset. Similarly, GB models tended to overfit small or noisy partitions, leading to inferior generalization performance. Therefore, the RF has shown better prediction performance for this dataset. In the case of the RF algorithm, Pearson's  $r$  values of specific capacitance, cyclic stability, and capacitive retention are found to be greater than 0.90. Moreover, the Adj.  $R^2$  values of the linear fitting of the scatter plots are found to be greater than 0.82 (Fig. 5a–f). This suggests that the RF algorithm achieved a high level of accuracy during the prediction of output performance features of MXene-based SCs. The predicted data observed in the scatter plots exhibit a strong linear relationship, with most of the data points closely fitting the model. The present finding suggested that the RF algorithm is effective in predicting the specific capacitance, cyclic stability, and capacitive retention of the MXene-based SCs. The RF algorithm, recognized for its ensemble learning approach, integrates multiple decision trees to enhance predictive accuracy and mitigate overfitting [39]. This method is well-suited for analyzing intricate relationships within electrochemical data, making it a valuable tool for performance prediction in energy storage applications [71].

#### 3.5. Experimental validation

The experimental validation of the ML results is an important step. Herein, we have validated the present ML results based on GCD and CV datasets by fabricating the MXene-based SCs. For this, the guidelines provided by the CART algorithm and feature importance results are taken into consideration. The detailed experimental conditions are provided in the supporting information file and in Tables S4 and S5. According to CART guidelines (Fig. 2), we fabricated NiFe-LDH/MXene electrodes and aimed to achieve a specific capacitance greater than 550 F/g. This performance can be obtained by fabricating WE excluding bare MXene, as well as metal-oxide/hydroxide-MXene, carbon-MXene, and polymer-MXene electrodes. Considering these factors, we have fabricated NiFe-LDH/MXene electrodes for SC application.

The structural, morphological, and electrochemical behavior of NiFe-LDH/MXene electrodes is shown in Fig. 6. The synthesized composite material is well-matched with the reported XRD pattern (Fig. 6a) [72]. In addition, the composite material shows all the characteristic



**Fig. 5.** Output performance features prediction of MXene-based SCs with the help of the RF algorithm (GCD and CV datasets). Prediction of (a) specific capacitance, (b) cyclic stability, and (c) capacitive retention based on the GCD dataset. Prediction of (d) specific capacitance, (e) cyclic stability, and (f) capacitive retention based on CV dataset. The data are fitted with a linear fitting method.

peaks of MXene and LDH. Although the position of the (200) peak is slightly shifted towards a lower angle, this indicates that the growth of LDH on the MXene sheet inhibits the aggregation of MXene. Simultaneously, the (003), (006), and (012) peaks are more prominent in the composite material than in pure LDH because LDH can better nucleate and grow on the MXene surface with high crystallinity. In the case of the Raman spectrum, the D and G bands indicate the presence of carbon-based elements in the sample. This indication is related to the presence of MXene in the sample (Fig. 6b). The scanning electron microscopy (SEM) image indicates that the sample has a layered sheet-like morphology (Fig. 6c). The CV and GCD plots of NiFe-LDH/MXene electrodes are shown in Fig. 6d and e, respectively. The CV and GCD plots demonstrate that the NiFe-LDH/MXene electrode has good supercapacitor performance. The specific capacitance of the NiFe-LDH/MXene electrode based on the GCD plot was found to be 543.41 F/g at a current density of 2 A/g. The target (ML prediction) capacitance was  $\geq 550$  F/g. This slight difference between experimental and ML prediction capacitance can be attributed to minor synthesis imperfections, such as variation in etching time and synthesis temperature, which may influence the surface terminations and active sites of MXene [73,74]. Additionally, certain unpredictable experimental factors including environmental humidity were not considered in the ML model which may also have contributed to the observed difference.

The electrochemical impedance spectrum (EIS) of the prepared electrode was measured at a frequency range of 100 kHz to 10 mHz with an AC amplitude of 10 mV. Fig. 6f illustrates the Nyquist plot, which consists of a semicircle in a high-frequency region and a linear response in a low-frequency region. The semicircle at high frequency acts as the internal resistance of the active material, ionic resistance of the electrolyte, and contact resistance in the electrode [75]. With the help of the Z-fit technique, an equivalent circuit was fitted to experimental EIS data. The corresponding equivalent circuit is shown in the inset of Fig. S8a. From the fitting results, the electrolytic resistance ( $R_s$ ) and charge transfer resistance ( $R_{ct}$ ) of fabricated electrodes were found to be 0.619  $\Omega$  and 15.54  $\Omega$ , respectively. Fig. 6g and h shows the capacitive and diffusion-driven contribution of the NiFe-LDH/MXene electrode at

various scan rates (1–5 mV/s). It is found that the diffusion-controlled mechanism dominates the charge storage behavior of the NiFe-LDH/MXene electrode. As the scan rate increases, the capacitive charge contribution increases while the diffusion charge contribution decreases. The dominance of the diffusion-controlled charge storage mechanism indicates that the fabricated electrode stores charge predominantly through a faradaic process rather than a non-faradic process [76,77]. The cyclic stability and coulombic efficiency are important indicators for identifying the performance of SC. In the present case, the cyclic stability of the electrodes was found to be 55.87 % after 5000 cycles, along with 92.33 % Coulombic efficiency (Fig. 6i). The degradation in the capacitance retention may be attributed to structural deformation and partial loss of active material during repeated charging-discharging cycles, which is common in LDH-based electrodes. However, initial high capacitance and good rate capability indicate strong redox activity and efficient ion transport [78,79].

In addition to this, we have experimentally validated the CV-based ML outcomes by fabricating the MoO<sub>3</sub>/MXene SC (Fig. 7). For this, a CV-based CART model and feature importance results are taken into consideration. To achieve specific capacitance up to 766 F/g, the CV dataset-based ML model suggested maintaining the PW between -1 to +1 V or -0.5 to +0.5 V, and the material needs to be deposited onto substrates like carbon, Ni foam, graphite, and stainless-steel or develop a free-standing film. Additionally, WE can be the metal oxides/hydroxides, polymers, and N-doped materials. The detailed ML-guided fabrication of MXene SCs based on the CV dataset is described in the supporting information file and Table S5. Moreover, a detailed explanation of structural, morphological, and electrochemical properties is described in the supporting information file and displayed in Fig. 7a-i and Figure S8b. In the present case, a specific capacitance of 561.64 F/g at a scan rate of 5 mV/s was achieved for the MoO<sub>3</sub>/MXene SC. The fabricated electrode exhibited an electrolyte resistance ( $R_s$ ) of 0.745  $\Omega$  and a charge transfer resistance ( $R_{ct}$ ) of 3.864  $\Omega$ . It is found that the capacitive-controlled mechanism dominates the charge storage behavior of the MoO<sub>3</sub>/MXene electrode. The MoO<sub>3</sub>/MXene SC can retain 87 % of capacitance and 95 % of Coulombic efficiency after 2500

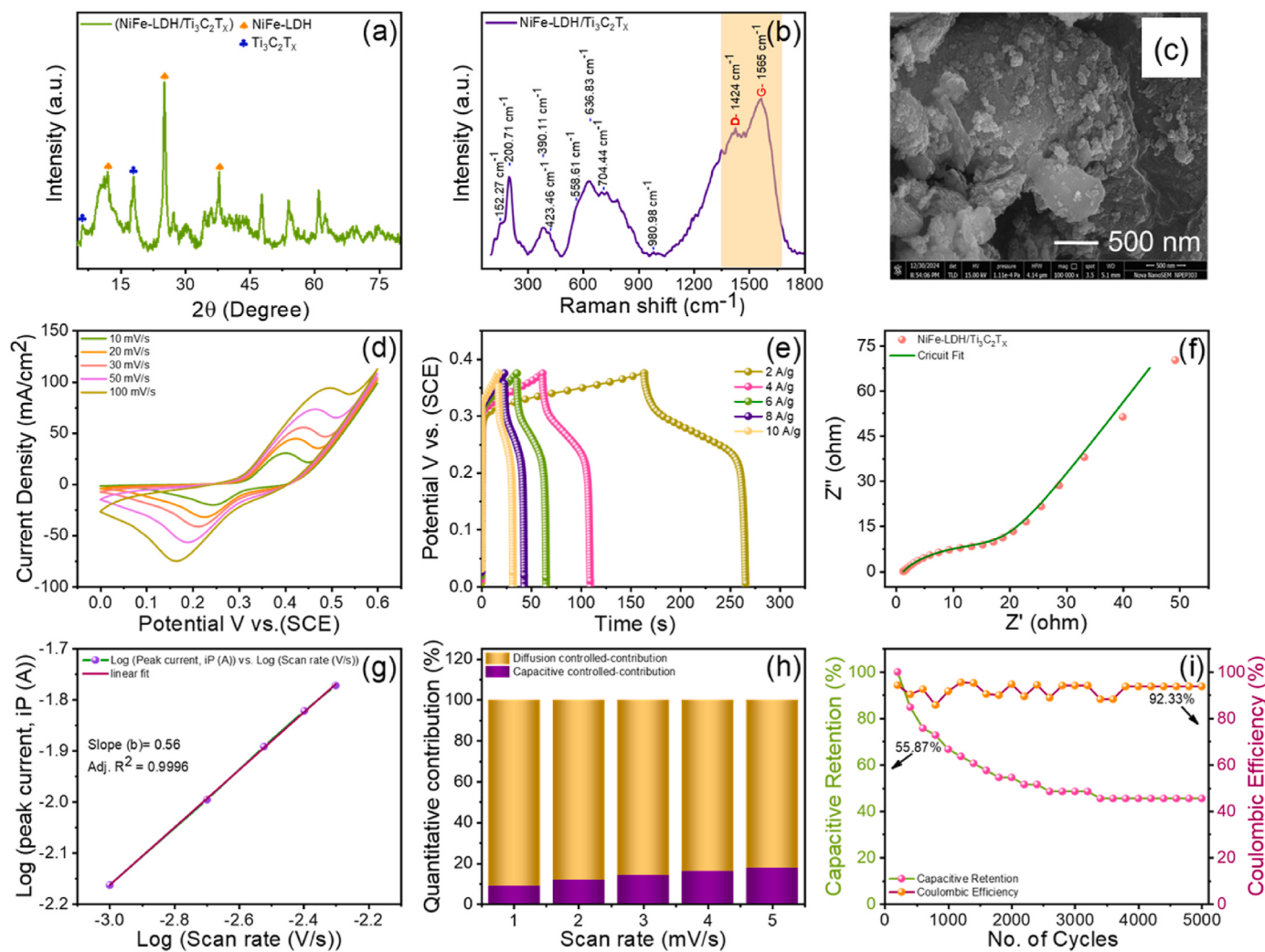


**Fig. 6.** Experimental validation of ML results by fabricating an MXene-based SC based on the GCD dataset. (a) XRD, (b) Raman, and (c) SEM results of the synthesized NiFe-LDH/MXene material. (d) CV, (e) GCD, (f) EIS results of the NiFe-LDH/MXene SC. (g–h) Capacitive and diffusion-driven contribution of the NiFe-LDH/MXene SC at various scan rates (1–5 mV/s) in 1M KOH electrolyte, (i) Capacitive Retention and Coulombic efficiency of NiFe-LDH/MXene SC.

cycles, suggesting good reliability for energy storage applications. Most of the experimental results of both SCs (NiFe-LDH/MXene and MoO<sub>3</sub>/MXene) are well-matched with GCD and CV-based ML outcomes.

#### 4. Conclusions

The present work demonstrates an ML-guided efficient approach for fabricating high-performance MXene-based SCs. The ML models constructed based on more than 7300 data points across 20 different parameters encompassing synthesis process, electrode/device fabrication, electrochemical parameter optimization, and SC output features, helped to build a robust design and prediction framework based on GCD and CV datasets. The CART algorithm provided valuable and predictive insights into improving specific capacitance, cyclic stability, and capacitive retention properties of the MXene-based SCs. In the case of predictions, the RF algorithm emerged as the most accurate for predicting output performance parameters of MXene-based SCs compared to GB, ANN, and LM algorithms. Additionally, the feature importance score highlighted how each input parameter affects the output performance of MXene-based SCs. Finally, ML insights and prediction results were experimentally validated by fabricating the NiFe-LDH/MXene and MoO<sub>3</sub>/MXene SCs. The experimental validation results are comparable with ML outcomes. In future studies, the MXene-based SCs could achieve higher specific capacitance by optimizing interlayer spacing and surface

terminations of the electrode materials. Additionally, incorporating conductive networks, suitable substrates, efficient electrode fabrication techniques, and optimized electrolytes further enhances the performance of MXene-based SCs. The MXene can be hybridized/composited with pseudocapacitive materials or conductive scaffolds. Such approaches can improve ion accessibility and charge transport, which significantly boosts the overall specific capacitance of MXene-based SCs. The present work provides a foundation for developing innovative strategies and guidelines for MXene-based SCs. The proposed ML approach is useful for accelerating the synthesis process, developing new SC electrodes, and optimizing various features of MXene-based SCs.

#### CRediT authorship contribution statement

**Anjali R. Shelake:** Writing – original draft, Visualization, Validation, Methodology, Investigation, Formal analysis, Data curation, Conceptualization. **Vijay C. Karade:** Visualization, Validation, Supervision, Formal analysis, Conceptualization. **Manickam Selvaraj:** Visualization, Resources, Funding acquisition, Formal analysis. **Mohammed A. Assiri:** Visualization, Resources, Funding acquisition, Formal analysis. **Dipti D. More:** Visualization, Methodology, Data curation. **Amruta D. Patil:** Visualization, Formal analysis, Data curation. **Mukund G. Mali:** Visualization, Resources, Formal analysis. **Santosh S. Sutar:** Validation, Software, Resources, Methodology, Formal analysis. **Rutuja**

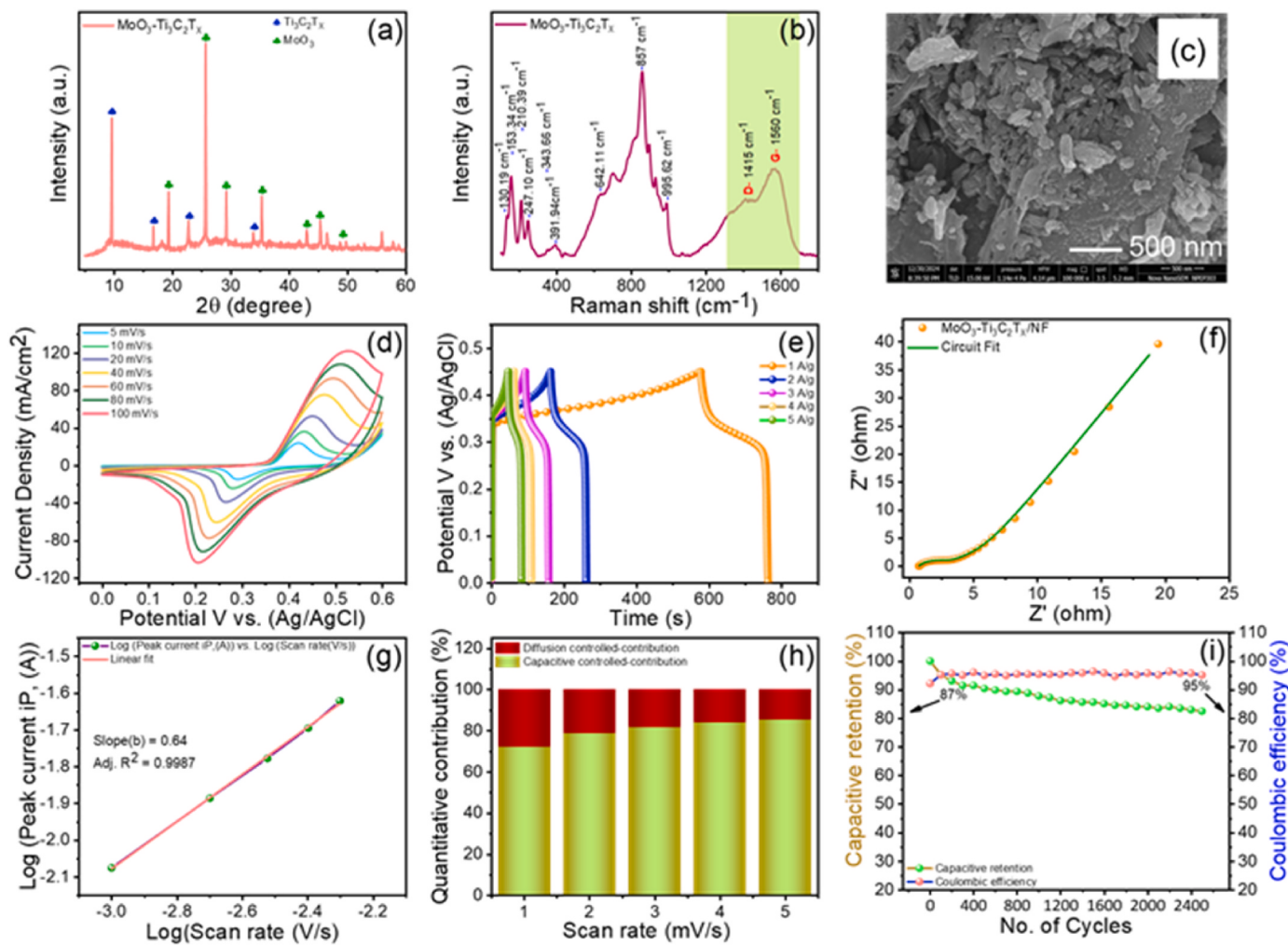


**Fig. 7.** Experimental validation of ML results by fabricating an MXene-based SC based on the CV dataset. (a) XRD, (b) Raman, and (c) SEM results of the synthesized  $\text{MoO}_3$ /MXene material. (d) CV, (e) GCD, (f) EIS results of the  $\text{MoO}_3$ /MXene SC. (g–h) Capacitive and diffusion-driven contribution of the  $\text{MoO}_3$ /MXene SC at various scan rates (1–5 mV/s) in 2M KOH electrolyte, (i) Capacitive retention and Coulombic efficiency of  $\text{MoO}_3$ /MXene SC.

**U. Amate:** Visualization, Resources, Investigation, Formal analysis, Conceptualization. **Chan-Wook Jeon:** Visualization, Resources, Project administration, Methodology, Formal analysis, Conceptualization. **Tae Geun Kim:** Visualization, Supervision, Resources, Project administration, Formal analysis, Conceptualization. **Tukaram D. Dongale:** Writing – review & editing, Visualization, Supervision, Resources, Project administration, Funding acquisition, Formal analysis, Conceptualization.

#### Declaration of competing interest

The authors declare that they have no known competing financial interests or personal relationships that could have appeared to influence the work reported in this paper.

#### Acknowledgments

The authors extend their appreciation to the Deanship of Scientific Research and Graduate Studies at King Khalid University for funding this work through the Large Project number, R.G.P. 2/742/46 and the authors acknowledge the Research Center for Advanced Materials (RCAMS) at King Khalid University, Saudi Arabia for their valuable technical support. ARS would like to thank the SARTHI, Government of Maharashtra, for providing the Chhatrapati Shahu Maharaj National Research Fellowship (CSMNRF-2023). TDD would like to thank RUSA-Research Fellowship (CSMNRF-2023).

Maharashtra for the financial assistance under the "RUSA-Industry Sponsored Centre for VLSI System Design."

#### Appendix A. Supplementary data

Supplementary data to this article can be found online at <https://doi.org/10.1016/j.jpowsour.2025.238863>.

#### Data availability

Data will be made available on request.

#### References

- [1] T.M. Gür, Review of electrical energy storage technologies, materials and systems: challenges and prospects for large-scale grid storage, *Energy Environ. Sci.* 11 (2018) 2696–2767, <https://doi.org/10.1039/C8EE01419A>.
- [2] A. Tyagi, K.M. Tripathi, R.K. Gupta, Recent progress in micro-scale energy storage devices and future aspects, *J. Mater. Chem. A* 3 (2015) 22507–22541, <https://doi.org/10.1039/C5TA05666G>.
- [3] R. Syamsai, A.N. Grace,  $\text{Ta}_4\text{C}_3$  MXene as supercapacitor electrodes, *J. Alloys Compd.* 792 (2019) 1230, <https://doi.org/10.1016/j.jallcom.2019.04.096>.
- [4] Z. Yu, L. Tetard, L. Zhai, J. Thomas, Supercapacitor electrode materials: nanostructures from 0 to 3 dimensions, *Energy Environ. Sci.* 8 (2015) 702–733, <https://doi.org/10.1039/C4EE03229B>.
- [5] T.M. Gür, Review of electrical energy storage technologies, materials and systems: challenges and prospects for large-scale grid storage, *Energy Environ. Sci.* 11 (2018) 2696–2767, <https://doi.org/10.1039/C8EE01419A>.

- [6] Z.S. Iro, C. Subramani, S.S. Dash, A brief review on electrode materials for supercapacitor, *Int. J. Electrochem. Sci.* 11 (2016) 10628–10643, <https://doi.org/10.20964/2016.12.50>.
- [7] H. Xia, J. Zhang, Z. Yang, S. Guo, S. Guo, Q. Xu, 2D MOF nanoflake-assembled spherical microstructures for enhanced supercapacitor and electrocatalysis performances, *Nano-Micro Lett.* 9 (2017) 43, <https://doi.org/10.1007/s40820-017-0144-6>.
- [8] R.K. Tripathy, A.K. Samantara, J.N. Behera, A cobalt metal-organic framework (Co-MOF): a bi-functional electro active material for the oxygen evolution and reduction reaction, *Dalton Trans.* 48 (2019) 10557, <https://doi.org/10.1039/C9DT01730E>.
- [9] C. Hao, B. Yang, F. Wen, J. Xiang, L. Li, W. Wang, Z. Zeng, B. Xu, Z. Zhao, Z. Liu, Y. Tian, Flexible all-solid-state supercapacitors based on liquid-exfoliated black-phosphorus nanoflakes, *Adv. Mater.* 28 (2016) 3194, <https://doi.org/10.1002/adma.201505730>.
- [10] C. Hu, E. Zhao, N. Nitta, A. Magasinski, G. Berdichevsky, G. Yushin, Aqueous solutions of acidic ionic liquids for enhanced stability of polyoxometalate-carbon supercapacitor electrodes, *J. Power Sources* 326 (2016) 569–574, <https://doi.org/10.1016/j.jpowsour.2016.04.036>.
- [11] R. Garg, A. Agarwal, M. Agarwal, A review on MXene for energy storage application: effect of interlayer distance, *Mater. Res. Express* 7 (2020) 022001, <https://doi.org/10.1088/2053-1591/ab750d>.
- [12] M. Naguib, M.W. Barsoum, Y. Gogotsi, Ten years of progress in the synthesis and development of MXenes, *Adv. Mater.* 33 (2021) 2103393, <https://doi.org/10.1002/adma.202103393>.
- [13] Y. Gogotsi, B. Anasori, The rise of MXenes, *J. Am. Chem. Soc.* 13 (2019) 8491–8494, <https://doi.org/10.1021/acsnano.9b06394>.
- [14] B. Xu, Y. Gogotsi, MXenes: from discovery to applications, *Adv. Funct. Mater.* 30 (2020) 1–3, <https://doi.org/10.1002/adfm.202007011>.
- [15] B. Anasori, Y. Gogotsi, MXenes: trends, growth, and future directions, *Graphene 2D Mater.* 7 (2022) 75–79, <https://doi.org/10.1007/s41127-022-00053-z>.
- [16] C.E. Shuck, A. Sarycheva, M. Anayee, A. Levitt, Y. Zhu, S. Uzun, V. Balitskiy, V. Zaborodina, O. Gogotsi, Y. Gogotsi, Scalable synthesis of Ti<sub>3</sub>C<sub>2</sub>T<sub>x</sub> MXene, *Adv. Eng. Mater.* 22 (2020) 1901241, <https://doi.org/10.1002/adem.201901241>.
- [17] J.C. Lei, X. Zhang, Z. Zhou, Recent advances in MXene: Preparation, properties, and applications, *Front. Phys.* 10 (2015) 276–286, <https://doi.org/10.1007/s11467-015-0493-x>.
- [18] S. Ali, M. Ahsan Farooq Qaisar, M. Sufyan Javed, K. Umer, S.S. Alarfaji, M. Mateen, M. Chhattal, S. Ali, A. Parkash, T. Lama Tamang, J. Qi, Two-dimensional MXene based innovative electrode materials for supercapacitors: recent advances and prospects, *Fuel* 377 (2024) 132783, <https://doi.org/10.1016/j.fuel.2024.132783>.
- [19] C. Zhan, M. Naguib, M. Lukatskaya, P.R.C. Kent, Y. Gogotsi, D.E. Jiang, Understanding the MXene pseudocapacitance, *J. Phys. Chem. Lett.* 9 (2018) 1223–1228, <https://doi.org/10.1021/acs.jpclett.8b00200>.
- [20] S. Ali, M. Sufyan Javed, K. Umer, J. Wang, Y. Fu, S. Kong, S. Khan, A. Ahmad, A. Parkash, M.D. Albaqami, Annu, J. Qi, D. He, Mo<sub>2</sub>@Ti<sub>3</sub>C<sub>2</sub>T<sub>x</sub> heterostructure: a new negative electrode material for Li-ion hybrid supercapacitors, *Chem. Eng. J.* 498 (2024) 155330, <https://doi.org/10.1016/j.cej.2024.155330>.
- [21] M.S. Alam, M.A. Chowdhury, T. Khandaker, M.S. Hossain, M.S. Islam, M.M. Islam, M.K. Hasan, Advancements in MAX phase materials: structure, properties, and novel applications, *RSC Adv.* 14 (2024) 26995–27041, <https://doi.org/10.1039/D4RA03714F>.
- [22] J. Li, X. Yuan, C. Lin, Y. Yang, L. Xu, X. Du, J. Xie, J. Lin, J. Sun, Achieving high pseudocapacitance of 2D titanium carbide (MXene) by cation intercalation and surface modification, *Adv. Energy Mater.* 7 (2017) 1602725, <https://doi.org/10.1002/aenm.201602725>.
- [23] A. Qian, J.Y. Seo, H. Shi, J.Y. Lee, C.H. Chung, Surface functional groups and electrochemical behavior in dimethyl sulfoxide-delaminated Ti<sub>3</sub>C<sub>2</sub>T<sub>x</sub> MXene, *ChemSusChem* 11 (2018) 3719–3723, <https://doi.org/10.1002/cscs.201801759>.
- [24] X. Zhan, C. Si, J. Zhou, Z. Sun, MXene and MXene-based composites: synthesis, properties and environment-related applications, *Nanoscale Horiz.* 5 (2020) 235–258, <https://doi.org/10.1039/C9NH00571D>.
- [25] S. De, S. Acharya, S. Sahoo, G.C. Nayak, Current trends in MXene research: properties and applications, *Mater. Chem. Front.* 5 (2021) 7134–7169, <https://doi.org/10.1039/DQMF00556A>.
- [26] D. Xiong, X. Li, Z. Bai, S. Lu, Recent advances in layered Ti<sub>3</sub>C<sub>2</sub>T<sub>x</sub> MXene for electrochemical energy storage, *Small* 14 (2018) 1703419, <https://doi.org/10.1002/smll.201703419>.
- [27] S. Ali, A. Ahmad, I. Hussain, S.S.A. Shah, S. Ali, A. Ali, M. Sufyan Javed, Experimental and theoretical aspects of MXenes-Based energy storage and energy conversion devices, *J. Chem. and Environ. 2* (2023) 54–81, <https://doi.org/10.56946/jce.v2i2.214>.
- [28] S. Ali, T. Ahmad, M.Y. Tahir, M. Usman, M. Chhattal, I. Hussain, S. Khan, A. M. Hassan, M.A. Assiri, P. Rosaiah, M.S. Javed, B. Akkinapally, J. Qi, The emergence of density functional theory for supercapacitors: recent progress and advances, *J. Energy Storage* 73 (2023) 109100, <https://doi.org/10.1016/j.est.2023.109100>.
- [29] S. Jha, M. Yen, Y.S. Salinas, E. Palmer, J. Villafuerte, H. Liang, Machine learning-assisted materials development and device management in batteries and supercapacitors: performance comparison and challenges, *J. Mater. Chem.* 11 (2023) 3904–3936, <https://doi.org/10.1039/D2TA07148G>.
- [30] N.C. Frey, J. Wang, G.I. Vega Bellido, B. Anasori, Y. Gogotsi, V.B. Shenoy, Prediction of synthesis of 2D metal carbides and nitrides (MXenes) and their precursors with positive and unlabeled machine learning, *ACS Nano* 13 (2019) 3031–3041, <https://doi.org/10.1021/acsnano.8b08014>.
- [31] G.J. Adekoya, O.C. Adekoya, U.K. Ugo, E.R. Sadiku, Y. Hamam, S.S. Ray, A mini-review of artificial intelligence techniques for predicting the performance of supercapacitors, *Mater. Today Proc.* 62 (2022) S184–S188, <https://doi.org/10.1016/j.matpr.2022.05.079>.
- [32] B. Mahesh, Machine learning algorithms - a review, *Int. J. Sci. Res.* 9 (2020) 381, <https://doi.org/10.21275/ART20203995>.
- [33] V. Sawant, R. Deshmukh, C. Awati, Machine learning techniques for prediction of capacitance and remaining useful life of supercapacitors: a comprehensive review, *J. Energy Chem.* 77 (2023) 438–451, <https://doi.org/10.1016/j.jecchem.2022.11.012>.
- [34] Z. Huang, J. Qin, Y. Zhu, K. He, H. Chen, H.Y. Hoh, M. Batmunkh, T.M. Benedetti, Q. Zhang, C. Su, S. Zhang, Y.L. Zhong, Green and scalable electrochemical routes for cost-effective mass production of MXenes for supercapacitor electrodes, *Carbon Energy* 5 (2023) e295, <https://doi.org/10.1002/cey.2295>.
- [35] W.Z. Tawfik, M.S. Abdel-Wahab, J.K. Lee, A.M. Al-Enizi, R.Y. Youssef, Modeling specific capacitance of carbon nanotube-based supercapacitor electrodes by machine learning algorithms, *Phys. Scripta* 99 (2024) 066011, <https://doi.org/10.1088/1402-4896/ad4df3>.
- [36] S. Krishna, A. Mir, Unlocking the potential of Ti<sub>3</sub>C<sub>2</sub> electrodes: a data-driven capacitance prediction study, *Energy Adv* 3 (2024) 2986–2998, <https://doi.org/10.1039/D4YA00460D>.
- [37] A. Zaheer, S.A. Zahra, M.Z. Iqbal, A. Mahmood, S.A. Khan, S. Rizwan, Nickel-adsorbed two-dimensional Nb<sub>2</sub>C MXene for enhanced energy storage applications, *RSC Adv.* 12 (2022) 4624, <https://doi.org/10.1039/D2RA00014H>.
- [38] B.M. Jun, S. Kim, J. Heo, C.M. Park, N. Her, M. Jang, Y. Huang, J. Han, Y. Yoon, Review of MXenes as new nanomaterials for energy storage/delivery and selected environmental applications, *Nano Res.* 12 (2019) 471–487, <https://doi.org/10.1007/s12274-018-2225-3>.
- [39] S.M. Patil, S.S. Kundale, S.S. Sutar, P.J. Patil, A.M. Teli, S.A. Beknalkar, R. K. Kamat, J. Bae, J.C. Shin, T.D. Dongale, Unraveling the importance of fabrication parameters of copper oxide-based resistive switching memory devices by machine learning techniques, *Sci. Rep.* 13 (2023) 4905, <https://doi.org/10.1038/s41598-023-32173-8>.
- [40] K.C. Tsay, L. Zhang, J. Zhang, Effects of electrode layer composition/thickness and electrolyte concentration on both specific capacitance and energy density of supercapacitor, *Electrochim. Acta* 60 (2012) 428–436, <https://doi.org/10.1016/j.electacta.2011.11.087>.
- [41] K. Lv, J. Zhang, X. Zhao, N. Kong, J. Tao, J. Zhou, Understanding the effect of pore size on electrochemical capacitive performance of MXene foams, *Small* 18 (2022) 2202203, <https://doi.org/10.1002/smll.202202203>.
- [42] S. De, C.K. Maity, M.J. Kim, G.C. Nayak, Tin(IV) selenide anchored-biowaste derived porous carbon-Ti<sub>3</sub>C<sub>2</sub>T<sub>x</sub> (MXene) nanohybrid: an ionic electrolyte enhanced high performing flexible supercapacitor electrode, *Electrochim. Acta* 463 (2023) 142811, <https://doi.org/10.1016/j.electacta.2023.142811>.
- [43] Q. Song, Z. Zhan, B. Chen, Z. Zhou, C. Lu, Biotemplate synthesis of polypyrrole@bacterial cellulose/MXene nanocomposites with synergistically enhanced electrochemical performance, *Cellulose* 27 (2020) 7475–7488, <https://doi.org/10.1007/s10570-020-03310-7>.
- [44] J.M. Goff, F.M. dos S. Vieira, N.D. Keilbart, Y. Okada, I. Dabo, Predicting the pseudocapacitive windows for MXene electrodes with voltage-dependent cluster expansion models, *ACS Appl. Energy Mater.* 4 (2021) 3151–3159, <https://doi.org/10.1021/acsaelm.0c02910>.
- [45] K. Shen, S. Zhai, S. Wang, Q. Ru, X. Hou, K. San Hui, K. Nam Hui, F. Chen, Recent progress in binder-free electrodes synthesis for electrochemical energy storage application, *Batteries Supercaps* 4 (2021) 860–880, <https://doi.org/10.1002/batt.202000271>.
- [46] M. Hashempour, A. Vicenzo, M. Bahdanchyk, M. Bestetti, Parameters influencing the capacitive behavior of carbon composite electrodes: composition, morphology, electrical conductivity, and surface chemistry, *J. Solid State Electrochem.* 22 (2018) 3895–3911, <https://doi.org/10.1007/s10008-018-4095-8>.
- [47] T. Wang, H.C. Chen, F. Yu, X.S. Zhao, H. Wang, Boosting the cycling stability of transition metal compounds-based supercapacitors, *Energy Storage Mater.* 16 (2019) 545–573, <https://doi.org/10.1016/j.ensm.2018.09.007>.
- [48] Y. Tang, J. Zhu, C. Yang, F. Wang, Enhanced capacitive performance based on diverse layered structure of two-dimensional Ti<sub>3</sub>C<sub>2</sub> MXene with long etching time, *J. Electrochem. Soc.* 163 (2016) A1975, <https://doi.org/10.1149/2.0921609jes>.
- [49] J. Yan, S. Li, B. Lan, Y. Wu, P.S. Lee, Rational design of nanostructured electrode materials toward multifunctional supercapacitors, *Adv. Funct. Mater.* 30 (2020) 1902564, <https://doi.org/10.1002/adfm.201902564>.
- [50] C. Ma, M. Ma, C. Si, X. Ji, P. Wan, Flexible MXene-based composites for wearable devices, *Adv. Funct. Mater.* 31 (2021) 2009524, <https://doi.org/10.1002/adfm.2020009524>.
- [51] R. Sinha, P. Kiran, K. Kumar, N. Pandit, C. Satish, S. Keshri, A. Keshri, MXene/biomass-Derived activated carbon composite for supercapacitor applications, *Carbon* 236 (2025) 120101, <https://doi.org/10.1016/j.carbon.2025.120101>.
- [52] J. Yang, W. Bao, P. Jaumaux, S. Zhang, C. Wang, G. Wang, MXene-based composites: synthesis and applications in rechargeable batteries and supercapacitors, *Adv. Mater. Interfaces* 6 (8) (2019) 1802004, <https://doi.org/10.1002/admi.201802004>.
- [53] W. Luo, Y. Ma, T. Li, H. Thabet, C. Hou, M. Ibrahim, S. El-Bahy, B. Xu, Z. Guo, Overview of MXene/conducting polymer composites for supercapacitors, *J. Energy Storage* 52 (2022) 105008, <https://doi.org/10.1016/j.est.2022.105008>.
- [54] Y. Gui, Q. Shi, Z. Liu, J. Lv, C. Wang, X. Xie, S. Zhang, MXene/biomass/chitosan carbon aerogel (MBC) with shared cathode and anode for the construction of high-efficiency asymmetric supercapacitor, *Chem. Eng. J.* 472 (2023) 144701, <https://doi.org/10.1016/j.cej.2023.144701>.

- [55] K. Chaudhary, S. Zulfiqar, K.M. Abualnaja, M. Shahid, H.M. Abo-Dief, M. Farooq Warsi, E.W. Cochran,  $Ti_3C_2Tx$  MXene reinforcement: a nickel-vanadium selenide/MXene based multi-component composite as a battery-type electrode for supercapacitor applications, *Dalton Trans* 53 (2024) 11147–11164, <https://doi.org/10.1039/d4dt01230e>.
- [56] L. Shi, R. Liu, Y. Tang, J. Wang, Z. Wang, G. Cheng, M. Hu, Y. Yang, J. Ding, Hollow porous  $Co_{0.85}Se/ZnSe@MXene$  anode with multilevel Built-in electric fields for high-performance sodium ion capacitors, *Inorg. Chem.* 63 (2024) 22923–22934, <https://doi.org/10.1021/acs.inorgchem.4c04021>.
- [57] A. Mendhe, H.S. Panda, A review on electrolytes for supercapacitor device, *Discov. Mater.* 3 (2023) 29, <https://doi.org/10.1007/s43939-023-00065-3>.
- [58] M. Sajjad, M.I. Khan, F. Cheng, W. Lu, A review on selection criteria of aqueous electrolytes performance evaluation for advanced asymmetric supercapacitors, *J. Energy Storage* 40 (2021) 102729, <https://doi.org/10.1016/j.est.2021.102729>.
- [59] D. Mandal, P. Routh, A.K. Mahato, A.K. Nandi, Electrochemically modified graphite paper as an advanced electrode substrate for supercapacitor application, *J. Mater. Chem. A* 7 (2019) 17547–17560, <https://doi.org/10.1039/C9TA04496E>.
- [60] V. Orts Mercadillo, K.C. Chan, M. Cairomi, A. Athanassiou, I.A. Kinloch, M. Bissett, P. Cataldi, Electrically conductive 2D material coatings for flexible and stretchable electronics: a comparative review of graphenes and MXenes, *Adv. Funct. Mater.* 32 (2022) 2204772, <https://doi.org/10.1002/adfm.202204772>.
- [61] Y. Liu, Y. Zhang, Z. Sun, S. Cheng, P. Cui, Y. Wu, J. Zhang, J. Fu, E. Xie, New insight into the mechanism of multivalent ion hybrid supercapacitor: from the effect of potential window viewpoint, *Small* 16 (2020) 2003403, <https://doi.org/10.1002/smll.202003403>.
- [62] N. Zarshad, A.U. Rahman, J. Wu, A. Ali, F. Raziq, L. Han, P. Wang, G. Li, H. Ni, Enhanced energy density and wide potential window for K incorporated  $MnO_2$ @carbon cloth supercapacitor, *Chem. Eng. J.* 415 (2021) 128967, <https://doi.org/10.1016/j.cej.2021.128967>.
- [63] Z. Zhu, S. Tang, J. Yuan, X. Qin, Y. Deng, R. Qu, G.M. Haarberg, Effects of various binders on supercapacitor performances, *Int. J. Electrochem. Sci.* 11 (2016) 8270–8279, <https://doi.org/10.20964/2016.10.04>.
- [64] R. Na, N. Lu, L. Li, Y. Liu, J. Luan, G. Wang, A robust conductive polymer network as a multi-functional binder and conductive additive for supercapacitors, *Chelectrochem* 7 (2020) 3056–3064, <https://doi.org/10.1002/celc.202000726>.
- [65] K.C. Tsay, L. Zhang, J. Zhang, Effects of electrode layer composition/thickness and electrolyte concentration on both specific capacitance and energy density of supercapacitor, *Electrochim. Acta* 60 (2012) 428–436, <https://doi.org/10.1016/j.electacta.2011.11.087>.
- [66] X. Su, J. Zhang, H. Mu, J. Zhao, Z. Wang, Z. Zhao, C. Han, Z. Ye, Effects of etching temperature and ball milling on the preparation and capacitance of  $Ti_3C_2$  MXene, *J. Alloys Compd.* 752 (2018) 32–39, <https://doi.org/10.1016/j.jallcom.2018.04.152>.
- [67] T.D. Dongale, K.P. Patil, S.R. Vanjare, A.R. Chavan, P.K. Gaikwad, R.K. Kamat, Modelling of nanostructured memristor device characteristics using artificial neural network (ANN), *J. Comput. Sci.* 11 (2015) 82–90, <https://doi.org/10.1016/j.jocs.2015.10.007>.
- [68] R. Chauhan, P. Dumka, D.R. Mishra, Modelling conventional and solar Earth still by using the LM algorithm-based artificial neural network, *Int. J. Ambient Energy* 43 (2022) 1389–1396, <https://doi.org/10.1080/01430750.2019.1707113>.
- [69] C. Bentéjac, A. Csörgő, G. Martínez-Muñoz, A comparative analysis of gradient boosting algorithms, *Artif. Intell. Rev.* 54 (2021) 1937–1967, <https://doi.org/10.1007/s10462-020-09896-5>.
- [70] S.M. Patil, S.S. Kundale, S.S. Sutar, P.J. Patil, A.M. Teli, S.A. Beknalkar, R. K. Kamat, J. Bae, J.C. Shin, T.D. Dongale, Unraveling the importance of fabrication parameters of copper oxide-based resistive switching memory devices by machine learning techniques, *Sci. Rep.* 13 (2023) 4905, <https://doi.org/10.1038/s41598-023-32173-8>.
- [71] S. Mishra, R. Srivastava, A. Muhammad, A. Amit, E. Chiavazzo, M. Fasano, P. Asinari, The impact of physicochemical features of carbon electrodes on the capacitive performance of supercapacitors: a machine learning approach, *Sci. Rep.* 13 (2023) 6494, <https://doi.org/10.1038/s41598-023-33524-1>.
- [72] H. Zhou, F. Wu, L. Fang, J. Hu, H. Luo, T. Guan, B.S. Hu, M. Zhou, Layered NiFe-LDH/MXene nanocomposite electrode for high-performance supercapacitor, *Int. J. Hydrogen Energy* 45 (2020) 13080–13089, <https://doi.org/10.1016/j.ijhydene.2020.03.001>.
- [73] P.E. Lokhande, U. Rednam, S. Khasim, T.A. Hamdalla, A. Vedpathak, D. Kumar, K. Singh, Etching duration as a key parameter for tailoring  $Ti_3C_2Tx$  MXene electrochemical properties, *J. Phys. Chem. Solid.* 207 (2025) 112902, <https://doi.org/10.1016/j.jpcs.2025.112902>.
- [74] V. dos Passos de Souza, L.M.G. da Silva, R.K. Nishihora, S.F. Santos, Influence of the synthesis protocol on the electrochemical properties of  $Ti_3C_2Tx$  MXene supercapacitor electrodes, *Surf. Coat. Technol.* 514 (2025) 132583, <https://doi.org/10.1016/j.surfcoat.2025.132583>.
- [75] H.S. Magar, R.Y.A. Hassan, A. Mulchandani, Electrochemical impedance spectroscopy (Eis): principles, construction, and biosensing applications, *Sensors* 21 (2021) 6578, <https://doi.org/10.3390/s21196578>.
- [76] S.S. Patil, J.C. Shin, P.S. Patil, Binder free hydrothermally synthesized nickel phosphate hydrate microplates on nickel foam for supercapacitors, *Ceram. Int.* 48 (2022) 29484–29492, <https://doi.org/10.1016/j.ceramint.2022.07.050>.
- [77] A.M. Teli, S.A. Beknalkar, D.S. Patil, S.A. Pawar, D.P. Dubal, V.Y. Burute, T. D. Dongale, J.C. Shin, P.S. Patil, Effect of annealing temperature on charge storage kinetics of an electrospun deposited manganese oxide supercapacitor, *Appl. Surf. Sci.* 511 (2020) 145466, <https://doi.org/10.1016/j.apsusc.2020.145466>.
- [78] T. Liu, H. Zhou, G. Zhong, X. Yan, X. Su, Z. Lin, Synthesis of NiFeAl LDHs from electroplating sludge and their excellent supercapacitor performance, *J. Hazard. Mater.* 404 (2021) 124113, <https://doi.org/10.1016/j.jhazmat.2020.124113>.
- [79] X. Wang, Y. Lin, Y. Su, B. Zhang, C. Li, H. Wang, L. Wang, Design and synthesis of ternary-component layered double hydroxides for high-performance supercapacitors: understanding the role of trivalent metal ions, *Electrochim. Acta* 225 (2017) 263–271, <https://doi.org/10.1016/j.electacta.2016.12.160>.